Experimental Study of the Eigenfrequency Shift Mechanism in a Blocked Pipe System

Moez Louati[1]; Silvia Meniconi[2]; Mohamed S. Ghidaoui, M.ASCE[3]; and Bruno Brunone, M.ASCE[4]

Downloaded from ascelibrary.org by Hong Kong University of Sci and Tech (HKUST) on 08/08/17. Copyright ASCE. For personal use only; all rights reserved.

Abstract: Eigenfrequency shift in a pipe with a blockage is investigated experimentally. The experimental test rig consists of a reservoir-pipe-valve (RPV) system that contains a single partial blockage. Blockages with different lengths are considered. The experiments confirm the existence of certain frequency bands where waves reflect strongly from the blockage and other bands where waves reflect weakly (Bragg-type resonance). These bands agree with the theoretically derived Bragg resonance condition. It is found that the values of the resonant frequencies are highly sensitive to the wave speed. For example, a 4% error in wave speed results in an error in the eigenfrequency estimates that increases almost linearly from approximately 4% for the first mode to 60% for the seventh mode. A direct and efficient approach is proposed for using the Bragg resonance condition to detect blockages in pipes. **DOI: 10.1061/(ASCE)HY.1943-7900.0001347.** © *2017 American Society of Civil Engineers.*

Author keywords: Bragg resonance; Blockage detection; Eigenfrequency shift; Pipe system; Transient wave.

Introduction

Like many municipal infrastructure systems, water supply systems (WSSs) are wasteful of both energy and water, with numerous malfunctioning devices and other undetected faults such as leakage, partially closed or closed valves, air blocks, and inefficient pump operation. These defects (sometimes) result in far less than optimal operation and performance, making these systems less sustainable by wasting both potable water and energy. The latter may also have a significant impact on the carbon footprint of water systems (Coelho and Andrade-Campos 2014; ASCE 2013; Colombo and Karney 2002).

One of the major factors contributing to the inefficient use of electrical or other power for operating both treatment plants and pumping stations in WSSs is pipe (or flow) blockage that occurs over their lifetime primarily due to physical or chemical processes [e.g., material deposition, tubercles (rust), scales, plaque, biofouling and inadvertently throttled inline valves, and air intrusion]. The buildup of material forming blockages on the inside of a pipe wall often begins in the form of increased wall roughness at small size, which grows with time and can eventually block a sizeable portion of the pipe's cross-sectional area. Such blockages increase pipe velocity and turbulent dissipation, resulting in potentially significant waste of energy and financial resources, reduction in carrying capacity, and increased potential for contamination. In addition, flow in severely blocked pipes can become throttled to such a degree that the flow may be redistributed in the pipe network, thereby reducing the system's overall redundancy (reliability). In some cases, overpressure of some pipes in the system occurs, increasing the potential for increased numbers of bursts and leakage. Whether for engineered or natural conduits, it is highly beneficial from both economic and environmental considerations to detect blockages so that they are dealt with in a timely manner.

In the last decade, transient test-based techniques have been used to detect partial blockages by injecting pressure waves and the analysis of the pressure signals has been executed in the time domain (e.g., Brunone et al. 2008a, b; Meniconi et al. 2016), frequency domain (e.g., Duan et al. 2011, 2013), and coupled time-frequency domains (Meniconi et al. 2013). Specifically, previous work in the frequency domain showed that the eigenfrequencies of a measured pressure signal vary with the cross-sectional area of the conduit (e.g., Duan et al. 2011; Qunli and Fricke 1990; Domis 1979, 1980; Schroeder 1967; Mermelstein 1967). Thus, the focus of past research has been on the inverse problem where mathematical relations linking the eigenfrequencies to the cross-sectional area of the pipe are formulated, and algorithms for evaluating blockage characteristics (location, length, size) from these relationships and measured eigenfrequencies were proposed (e.g., Duan et al. 2011, 2013; Stephens 2008; De Salis and Oldham 1999; Schroeter and Sondhi 1994; Qunli and Fricke 1989, 1990; Milenkovic 1984, 1987; Sondhi and Resnick 1983; Domis 1980, 1979; Fant 1975; Sondhi and Gopinath 1971; Heinz 1967; Mermelstein 1967; Schroeder 1967).

While this research direction has produced promising results and has led to proof of concept under idealized laboratory settings, there are a number of unresolved issues. For example, there is neither a proof that the inverse problem, which relates the unknown blockage properties to the measured eigenfrequencies, has a unique solution nor is there a technique to find it even if it would exist. In fact, currently proposed solutions of this inverse problem require that the number of blockages is known a priori, which is unrealistic in practice. In addition, the computational time needed to solve the inverse problem grows exponentially with the number of blockages, and the accuracy of the developed techniques is still low.

[1]Postdoctoral Fellow, Dept. of Civil and Environmental Engineering/School of Engineering, Hong Kong Univ. of Science and Technology, Kowloon, Hong Kong (corresponding author). E-mail: mlouati@ust.hk

[2]Associate Professor, Dept. of Civil and Environmental Engineering, Univ. of Perugia, 06125 Perugia, Italy. E-mail: silvia.meniconi@unipg.it

[3]Chair Professor, Dept. of Civil and Environmental Engineering/School of Engineering, Hong Kong Univ. of Science and Technology, Kowloon, Hong Kong. E-mail: ghidaoui@ust.hk

[4]Professor, Dept. of Civil and Environmental Engineering, Univ. of Perugia, 06125 Perugia, Italy. E-mail: bruno.brunone@unipg.it

Note. This manuscript was submitted on November 3, 2016; approved on March 16, 2017; published online on August 4, 2017. Discussion period open until January 4, 2018; separate discussions must be submitted for individual papers. This paper is part of the ***Journal of Hydraulic Engineering***, © ASCE, ISSN 0733-9429.

Earlier research work (Louati and Ghidaoui 2016a, b; Louati et al. 2016; Stevens 1998; El-Rahed and Wagner 1982) focused on studying the forward approaches such as understanding the mechanism causing the variation of the eigenfrequencies due to the presence of blockage in a bounded pipe system. The impetus for this direction of research is based on the premise that, if this forward problem is better understood, then ways to address the difficulties that arise from its inversion can be found.

This paper reviews the basic theoretical features of the eigenfrequency shift mechanism discussed in Louati and Ghidaoui (2016a, b) and Louati et al. (2016), and conducts experimental tests to validate these features. In particular, the effect of Bragg resonance on the eigenfrequency shift (Louati et al. 2016) is validated, and it is shown that the identification of such effects provides information on the blockage characteristics. Moreover, the relations that link the measured zero shifts as well as maximum shifts (i.e., significant shifts) to the blockage location (Louati and Ghidaoui 2016b) are also validated.

Brief Review of Eigenfrequency Shift Mechanism

For an intact reservoir-pipe-valve (RPV) system with pipe length L, the eigenfrequencies (natural resonant frequencies) are given by the following dispersion relation (Chaudhry 2014):

$$\cos(k_m^0 L) = 0 \Rightarrow w_m^0 = a k_m^0 = 2\pi\left[(2m-1)\frac{a}{4L}\right]; \qquad m \in Z^+ \tag{1}$$

where $k_m^0 = w_m^0/a$ = mth wave number; w_m^0 = mth eigenfrequency; and the superscript 0 = intact case.

It is shown that a variation in the cross-sectional area of a pipe shifts the eigenfrequencies (e.g., Duan et al. 2011; Schroeder 1967; Domis 1979). This eigenfrequency shift is used as key input information to determine the cross-sectional area distribution along the pipe using optimization techniques (e.g., Duan et al. 2011) or approximated area function (e.g., Mermelstein 1967; Qunli and Fricke 1990).

Consider a RPV system with a single blockage as shown in Fig. 1. The blocked pipe system is modeled as the junction of three pipes in series with different diameters (Fig. 1). The three pipes are defined as Pipe 1 with length l_1 and cross-sectional area $A_1 = A_0$; Pipe 2 with length l_2 and cross-sectional area $A_2 < A_0$; and Pipe 3 with length l_3 and cross-sectional area $A_3 = A_0$, where A_0 is the intact cross-sectional area. The ratio of the cross-sectional areas is $\alpha = A_2/A_0$ and the dimensionless lengths are defined by x/L, $\eta_1 = l_1/L$, $\eta_2 = l_2/L$, and $\eta_3 = l_3/L$, where $L = l_1 + l_2 + l_3$ is the total length of the blocked pipe system and x is the distance along the pipe length from the reservoir (Fig. 1). The pipe flow is assumed to be one-dimensional and frictionless. In what follows, the case without blockage (i.e., $\alpha = 1$) is referred to as the intact pipe case.

The dispersion relation that governs the eigenfrequencies of the blocked pipe system (Fig. 1) is given by El-Rahed and Wagner (1982) and Duan et al. (2011)

$$\begin{aligned}&\alpha\cos(k_m l_1)\cos(k_m l_2)\cos(k_m l_3)\\&-\cos(k_m l_1)\sin(k_m l_2)\sin(k_m l_3)\\&-\alpha^2\sin(k_m l_1)\sin(k_m l_2)\cos(k_m l_3)\\&-\alpha\sin(k_m l_1)\cos(k_m l_2)\sin(k_m l_3) = 0\end{aligned} \tag{2}$$

which could also be written as

$$\begin{aligned}&\cos(k_m L) + \frac{(1-\alpha)}{(1+\alpha)}\cos[k_m(l_1 - l_2 - l_3)]\\&-\frac{(1-\alpha)}{(1+\alpha)}\cos[k_m(l_1 + l_2 - l_3)]\\&-\frac{(1-\alpha)^2}{(1+\alpha)^2}\cos[k_m(l_1 - l_2 + l_3)] = 0\end{aligned} \tag{3}$$

where the subscript $m = m$th natural resonant mode; and $k_m = w_m/a$ = mth wave number, where $w_m = m$th eigenfrequency; and a = acoustic wave speed. When $\alpha = 1$, Eq. (3) becomes identical to the dispersion relation of the intact pipe case in Eq. (1).

The eigenfrequencies of the blocked pipe system are obtained by solving Eq. (3) graphically. Figs. 2 and 3 show the eigenfrequency (w_m) variation with length $\eta_b = \eta_3 + 0.5\eta_2$ for the first five modes and different α values when $\eta_2 = 0.15$ and $\eta_2 = 0.027$, respectively. The cases where $\alpha = 1$ in Figs. 2 and 3 represent the eigenfrequencies of the intact pipe case, which are constant and vary as straight horizontal line with $\eta_b = \eta_3 + 0.5\eta_2$. When $\alpha \neq 1$, the effect of the blockage is introduced, and as a result, the eigenfrequency at a given mode m (w_m) deviates from the intact case (w_m^0) as observed in Figs. 2 and 3. The eigenfrequency shift is defined as $\Delta w_m = (w_m - w_m^0)$, which could take positive, negative, or zero values (Figs. 2 and 3).

In previous research, blockage detection methods based on the eigenfrequency shifts are developed. These methods lack the use of information of the shift sign and how such shift occurs. In fact,

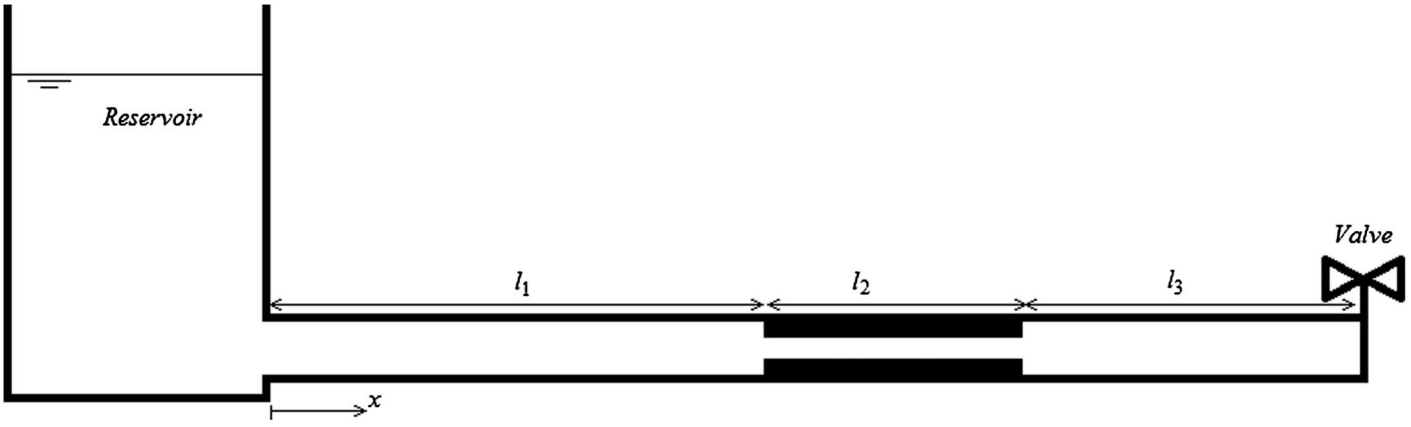

Fig. 1. Single blockage in a reservoir-pipe-valve system (bounded system)

Downloaded from ascelibrary.org by Hong Kong University of Sci and Tech (HKUST) on 08/08/17. Copyright ASCE. For personal use only; all rights reserved.

Downloaded from ascelibrary.org by Hong Kong University of Sci and Tech (HKUST) on 08/08/17. Copyright ASCE. For personal use only; all rights reserved.

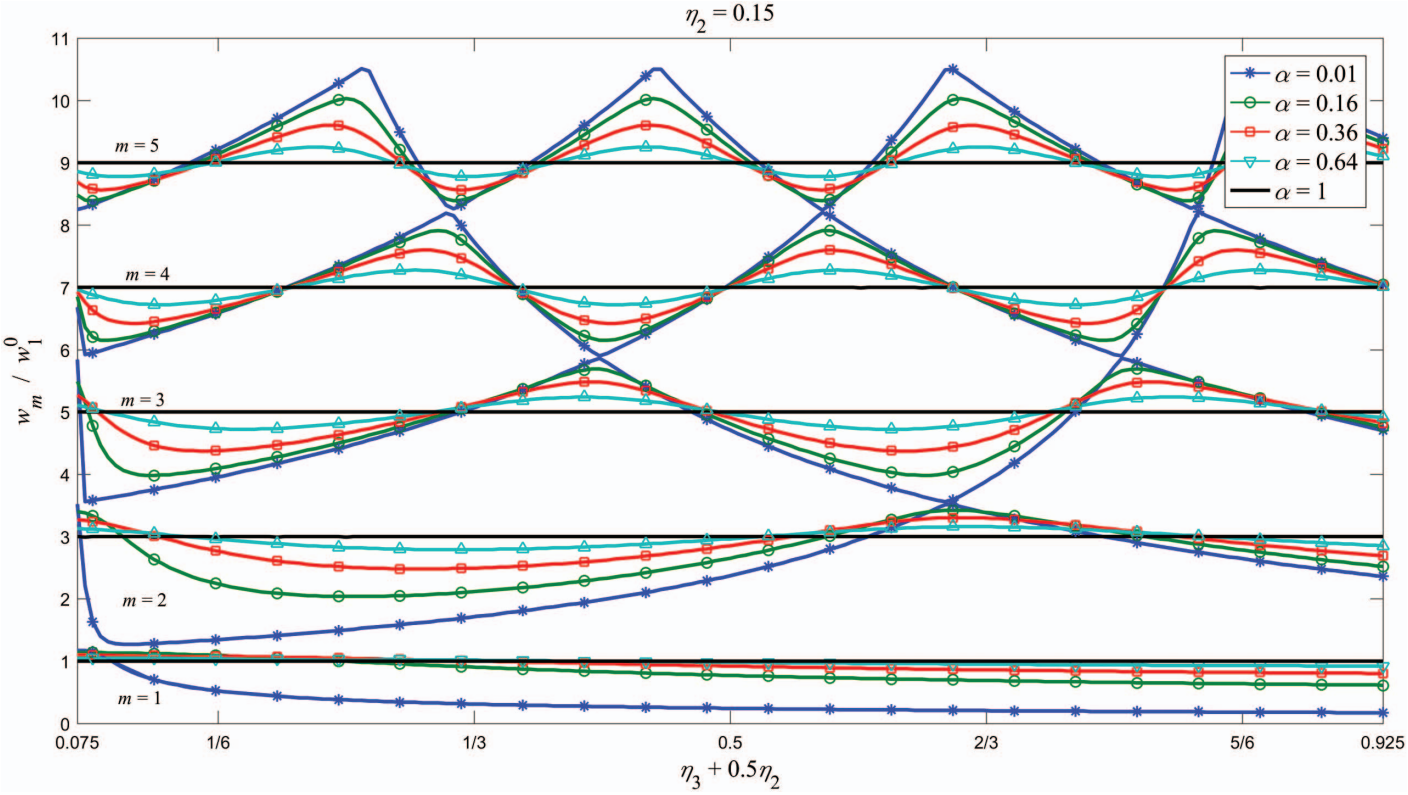

Fig. 2. (Color) Normalized eigenfrequency variation with length $\eta_b = \eta_3 + 0.5\eta_2$ of the first five modes for different α values when $\eta_2 = 0.15$ (Louati and Ghidaoui 2016b)

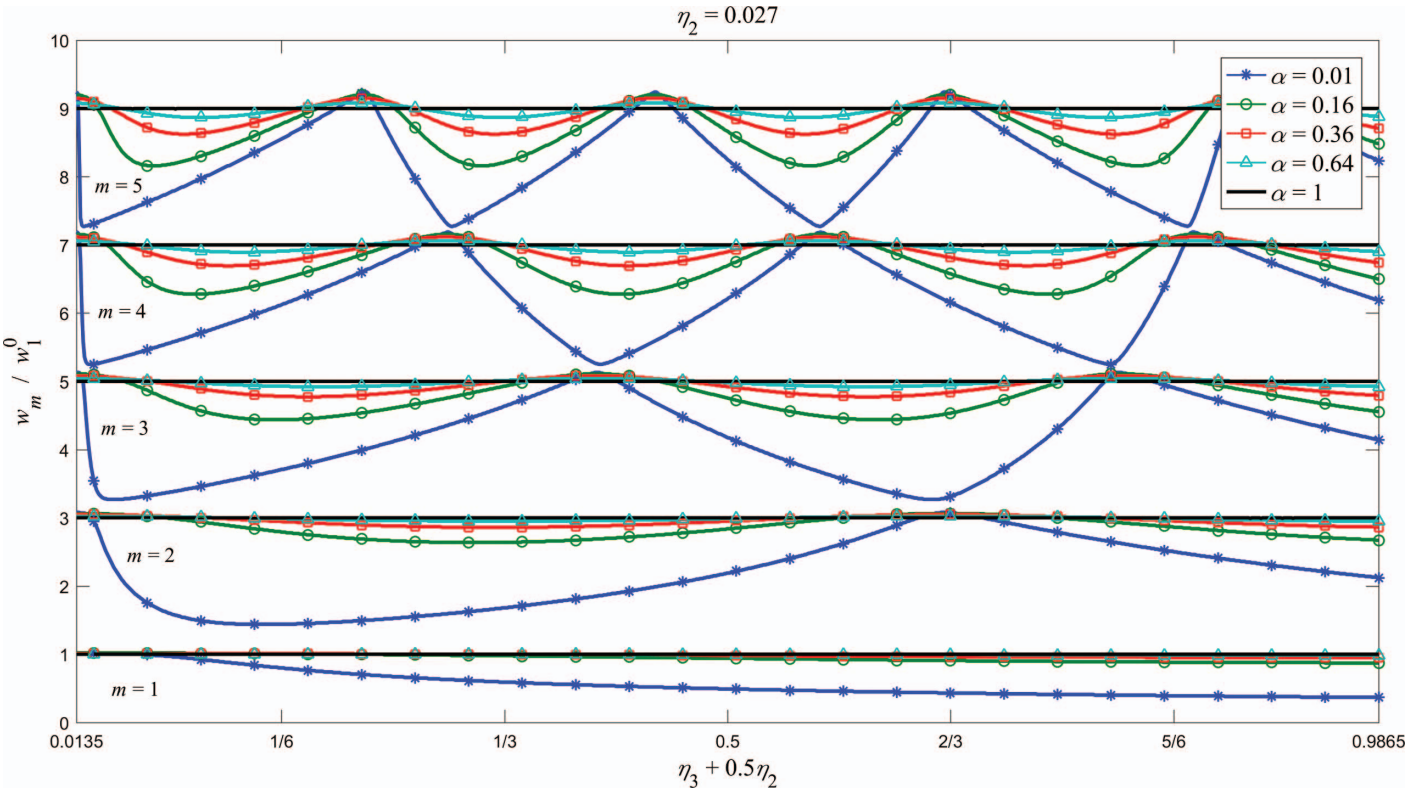

Fig. 3. (Color) Normalized eigenfrequency variation with length $\eta_b = \eta_3 + 0.5\eta_2$ of the first five modes for different α values when $\eta_2 = 0.027$ (Louati and Ghidaoui 2016b)

these methods are still not accurate and there is no proof that these methods provide a unique solution. A key advantage from understanding the shift mechanism is that it offers additional information that improves the accuracy and convergence of current blockage detection.

Bragg Resonance Frequencies

Having an acoustic wave source at the downstream boundary of a blocked pipe system (Fig. 1) as the frequency of these generated waves varies, Bragg resonance describes the mechanism of which waves reflect least and which waves reflect most toward the source. The frequencies at which maximum reflection and maximum transmission occur are called Bragg resonance frequencies and they are respectively given by Louati et al. (2016)

$$\cos(kl_2) = 0 \Rightarrow w_n^R(l_2) = 2\pi\left[(2n-1)\frac{a}{4l_2}\right]; \qquad n = 1, 2, 3 \tag{4}$$

and

$$\sin(kl_2) = 0 \Rightarrow w_n^T(l_2) = 2\pi\left[2(n-1)\frac{a}{4l_2}\right]; \qquad n = 1, 2, 3 \tag{5}$$

Eq. (4) indicates that if the blockage length (l_2) is an odd multiple of the quarter-wavelength, then maximum wave reflection from the blockage occurs. On the other hand, Eq. (5) indicates that if the blockage length (l_2) is a multiple of the half-wavelength, then the injected wave is totally transmitted through the blockage. Eq. (5) is valid for $n = 1$, however generating a wave with frequency $w = w_1^T = 0$ is physically impossible.

It is shown (Louati 2016; Louati et al. 2016) that at modes with eigenfrequencies close or equal to the Bragg resonance frequencies of total transmission, the blocked pipe system behaves similarly to an intact pipe system, and therefore small or no eigenfrequency shift is observed at those modes. In addition, at modes with eigenfrequencies close or equal to the Bragg resonance frequencies of maximum reflection, the blocked pipe system behaves similarly to a blocked pipe system with a blockage at the boundary with squared area ratio, and therefore large eigenfrequency shift is observed at those modes (Louati 2016; Louati et al. 2016). The eigenfrequency shift mechanism of a blocked pipe system with a blockage at the boundary was investigated in Louati and Ghidaoui (2016b), where it is shown that the area ratio for such system is given by

$$\sin\left(\frac{w_m^{\max}}{w_1^0}\frac{\pi}{2}\right) \pm \frac{1-\alpha^2}{1+\alpha^2} = 0 \Rightarrow \alpha = \sqrt{\frac{1 \mp \sin\left[\frac{w_m^{\max}}{w_1^0}\frac{\pi}{2}(1-\eta_2)\right]}{1 \pm \sin\left[\frac{w_m^{\max}}{w_1^0}\frac{\pi}{2}(1-\eta_2)\right]}} \le 1 \tag{6}$$

Therefore, Eq. (6) could be used at modes with eigenfrequencies close to w_n^R. Figs. 4 and 5 give the eigenfrequency variation obtained from Eq. (3) for the cases where $\eta_2 = 0.15$ and $\eta_2 = 0.027$, respectively, and where $\alpha = 0.16$ for both cases. Figs. 4 and 5 show the effect of Bragg resonance on the eigenfrequency variation at different modes as discussed previously. The axis of the blockage location in Fig. 5 is shortened to $1/3 \le \eta_3 + \eta_2/2 \le 2/3$ only for clarity of the curves.

In "Experimental Validation and Discussion of Eigenfrequency Shift Mechanism," it is shown how Bragg resonance frequencies could be identified from the measured frequency response function (FRF).

Zero Eigenfrequency Shift

Zero eigenfrequency shift occurs when the blockage location is as follows (Louati and Ghidaoui 2016b):

$$\eta_3 + \frac{\eta_2}{2} = \frac{2\bar{m} - \frac{2}{\pi}\arccos\left\{(-1)^{\bar{m}}\frac{(1-\alpha)}{(1+\alpha)}\cos[(2\ m-1)\frac{\pi}{2}\eta_2]\right\}}{2(2\ m-1)} \tag{7}$$

Eq. (7) gives the zero-shift locations ($\bar{m}$) at a given mode m and for a given area ratio α. For the case of shallow blockage case (i.e., $\alpha \approx 1$), Eq. (7) becomes

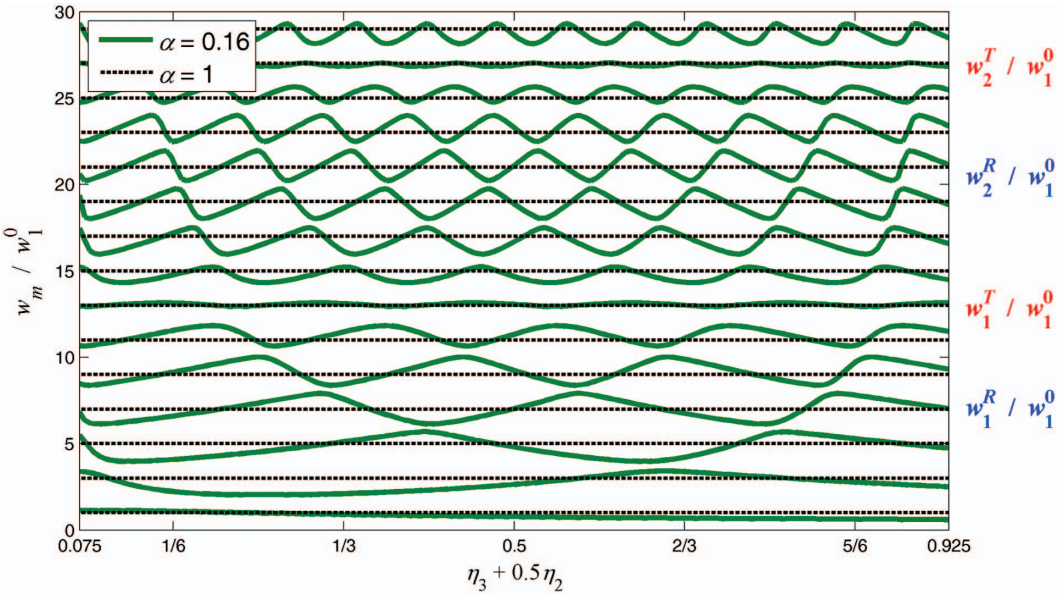

Fig. 4. (Color) Normalized eigenfrequency variation with length $\eta_b = \eta_3 + 0.5\eta_2$ of the first 15 modes when $\alpha = 0.16$ and $\eta_2 = 0.15$ (Louati et al. 2016)

J. Hydraul. Eng., 2017, 143(10): 04017044

Downloaded from ascelibrary.org by Hong Kong University of Sci and Tech (HKUST) on 08/08/17. Copyright ASCE. For personal use only; all rights reserved.

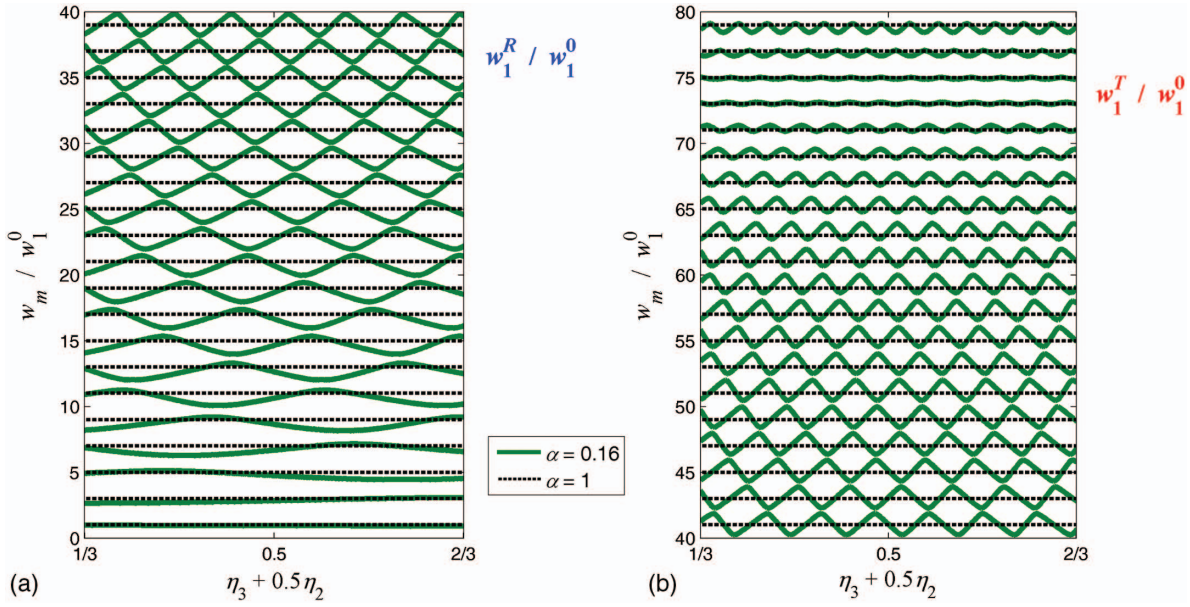

Fig. 5. (Color) Normalized eigenfrequency variation with length $\eta_b = \eta_3 + 0.5\eta_2$ when $\alpha = 0.16$ and $\eta_2 = 0.027$ for (a) the first 20 modes; (b) modes $m = 21$ to $m = 40$ (Louati et al. 2016)

$$\eta_3 + \frac{\eta_2}{2} = \frac{2\bar{m} - 1}{2(2m - 1)} \tag{8}$$

which is independent of area ratio (α). Notice that when

$$\cos[(2m - 1)\pi\eta_2/2] = 0 \tag{9}$$

which gives the Bragg resonance condition for maximum reflection [Eq. (4)], Eq. (7) becomes Eq. (8). This means that the zero-shift locations become independent of α at modes where $w_m \approx w_{\bar{m}}^R$ [Eq. (4)]. The deviation range of Eq. (7) from Eq. (8) is

$$\left[\frac{-1}{2(2m - 1)} \text{ to } \frac{1}{2(2m - 1)}\right] \tag{10}$$

These deviations become very small at high modes. Therefore Eq. (7) could be approximated by Eq. (8) at relatively high modes ($m > 3$).

Maximum Eigenfrequency Shift

The blockage location is related to the maximum eigenfrequencies ($w_m^{\max}$) as follows (Louati and Ghidaoui 2016b):

$$\eta_3 + \frac{\eta_2}{2} = \frac{1}{2}\left[1 - \frac{2(m - \bar{m}) - 1}{w_m^{\max}/w_1^0}\right]; \quad \text{with} \begin{cases} \frac{\eta_2}{2} < \eta_3 + \frac{\eta_2}{2} < 1 - \frac{\eta_2}{2} \\ \bar{m} \in Z^+ \end{cases} \tag{11}$$

The distinction between maximum (i.e., positive shift) and minimum (i.e., negative shift) eigenfrequency magnitudes is governed by Louati and Ghidaoui (2016b)

$$(-1)^{n_T + \bar{m}} \begin{cases} \text{if} > 0 \Rightarrow \text{maximum shift is negative} \\ \text{if} < 0 \Rightarrow \text{maximum shift is positive} \end{cases} \tag{12}$$

where n_T = integer that gives the number of modes region between two consecutive Bragg resonance frequencies of total transmission defined as

$$n_T = \text{Floor}\left[(2m - 1)\frac{\eta_2}{2}\right] + 1 \tag{13}$$

where Floor = function that gives the largest previous integer.

Low-Frequency Approximation

The first eigenfrequency could be approximated by Louati and Ghidaoui (2016a)

$$\frac{w_1}{w_1^0} \approx \frac{2}{\pi}\sqrt{\frac{\alpha}{\alpha^2\eta_1\eta_2 + \alpha\eta_1\eta_3 + \eta_2\eta_3}} \tag{14}$$

For severe blockage case (i.e., $\alpha \ll 1$), Eq. (14) becomes (Louati and Ghidaoui 2016b)

$$\frac{w_1}{w_1^0} \approx \frac{2}{\pi}\sqrt{\frac{\alpha}{\eta_2\eta_3}} \tag{15}$$

This is identical to the natural frequency of the Helmholtz resonator system (Stevens 1998). For short blockage case (Fig. 3), the shift is almost always nearly zero at the lowest mode ($m = 1$). Therefore, a significant shift of the lowest eigenfrequency is a good indication of severe blockage case where Eq. (15) or Eq. (14) could be used.

Experimental Validation and Discussion of Eigenfrequency Shift Mechanism

This section discusses the experimental validation of the properties of the eigenfrequency shift mechanism reviewed in the previous section.

Experimental Setup

The experimental investigation is carried out at the Water Engineering Laboratory of the University of Perugia, Italy. The two experimental setups consist of a RPV system that contains a single partial blockage as shown in Fig. 1; the blockage is simulated by means of

Downloaded from ascelibrary.org by Hong Kong University of Sci and Tech (HKUST) on 08/08/17. Copyright ASCE. For personal use only; all rights reserved.

Table 1. Main Characteristics of the Experimental Tests

Parameter	Setup 1	Setup 2
l_1 (m)	52.86	52.86
l_2 (m)	24	3.6
l_3 (m)	76.75	76.75
L (m)	153.61	133.21
$\eta_2 = l_2/L$	≈0.156	≈0.027
$D_1 = D_0$ (m)	0.0933	0.0933
D_2 (m)	0.0383	0.0383
$D_3 = D_0$ (m)	0.0933	0.0933
$\alpha = D_2^2/D_0^2$	0.168	0.168
Pipe wall thickness (m)	0.0167	0.0167
Wave speed (a) (m/s)	≈355 ± 15	≈355 ± 15

a small bore pipe with a diameter $D_2 < D_0$, where D_0 is the diameter of the blockage-free pipe and two different lengths l_2: for Setup 1, $l_2 = 24$ m as in the case shown in Fig. 4, and for Setup 2, $l_2 = 3.6$ m, as shown in Fig. 5. All pipes are horizontal high-density polyethylene (HDPE) pipes (Meniconi et al. 2011a, b). The main characteristics of the experimental setup are listed in Table 1.

In these experiments, an air vessel is used as a supply tank. To maintain the value of the supply pressure head, $H_{ST} \approx 10 \pm 1$ m, one of three submerged pumps placed in a recycling tank is used. Due to limited space in the laboratory, it is not possible to use a long, straight, pipe runs; therefore, a circular pipe setup with long radius bends is used. A schematic depiction of the experimental pipe setup is shown in Fig. 6, and part of the laboratory pipe setup is shown in Fig. 7.

Probing transients are generated using a portable pressure wave maker (PPWM) device, which can be used to generate sharp pressure waves of small amplitude (Brunone et al. 2008a, b; Meniconi et al. 2011a, b). The PPWM consists of a cylindrical steel pressure vessel with a diameter of 0.45 m and a total volume of approximately 0.20 m^3. A small-diameter, initially closed electrovalve (EV) connects the device to the test pipe as shown in Fig. 8. The diameter of the electrovalve is 6.35×10^{-3} m (1/4 in.). The small size of the valve allows the PPWM to be attached to the pipe using a simple fitting and also improves pressure signal quality. When being connected to potable water systems, the PPWM device must be carefully disinfected, cleaned, and filled with water from the test pipe. A piezometer is installed on the pressure vessel to visually monitor the water level and air volume in the device.

Pressure signals are measured using piezoresistive transducers with a full-scale range of 0.2 MPa (2 bar) to minimize reading error of the small pressures generated during the transient tests. The maximum measurement error was rated at ±0.15% of full scale and the transducer response time is approximately 1 ms. To minimize electronic noise, the pressure transducers are powered by 24 V direct current batteries. Calibration of pressure transducers (Measurements Specialties, Hampton, Virginia) is checked by means of a pressure calibrator in accordance with European Guidelines on the Calibration of Electromechanical Manometers by European co-operation for Accreditation (EA) (EURAMET 2011) confirming the data in the manufacturer's certificate. Pressures are sampled at a frequency of 1,024 Hz using a National Instruments (Austin, Texas) USB-6008 data acquisition system (DAQ) with a maximum analogue input single-channel sampling rate of 10 kS/s. In all tests, pressure signals are acquired simultaneously at three separate locations (T1, T2, and T3 in Fig. 6).

Before opening the PPWM connection valve, the initial conditions (subscript 0) in the test pipeline are the static pressure conditions in the pipe, where $H_{T1,0} = H_{T2,0} = H_{T3,0} = H_{ST}$; and $H_{P,0} \approx 43$ m in the PPWM.

The opening and subsequent closure of the EV is governed by an actuator and programmable controller to generate the desired waveform. In these experiments, an approximately square pulse waveform is generated and is created by a rapid opening and closing of the EV, with a wave-pulse duration $t_p = 50$ ms.

Fig. 9 shows a typical differential pressure signal referenced to the initial hydrostatic conditions and acquired at the various measurement sections during the pulse-generating valve maneuver in Setup 1. To calculate pressure wave speed, a, the distance between Sections T1 and T2 is divided by the time interval, Δt_{12}, that it takes for the pressure pulse to travel the length of the pipe section between the two transducer locations (Fig. 9).

For each setup, the same test is repeated eight times to check repeatability of the experiments and obtain an averaged wave speed value.

The pressure signals are analyzed in the frequency domain after being processed using the fast Fourier transform implemented in *MATLAB*. To provide a baseline modeling reference, the same transient in an elastic straight pipe with the same partial blockage

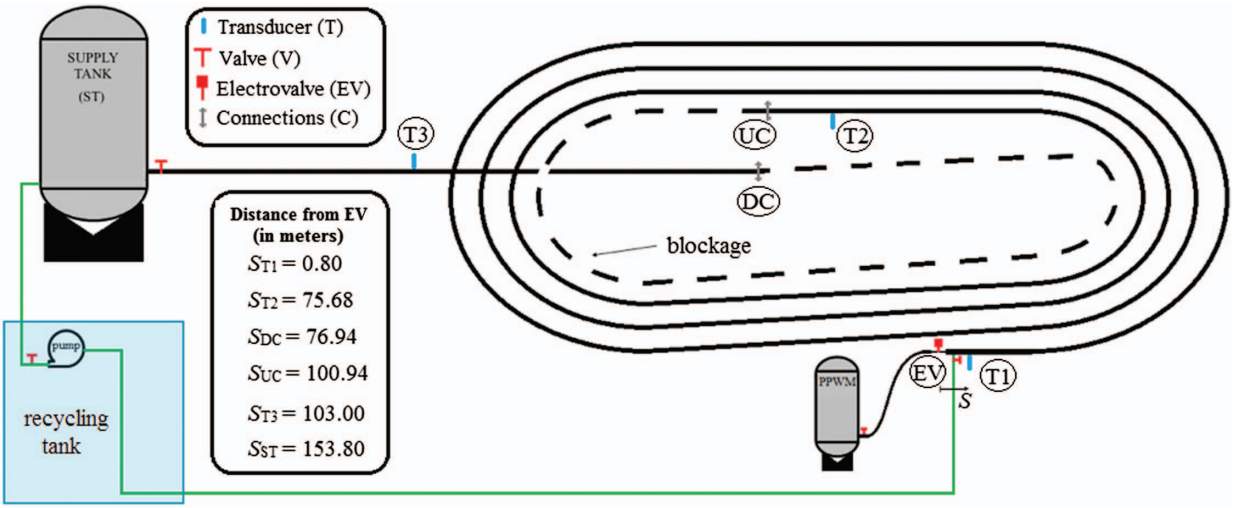

Fig. 6. (Color) Schematic of the intact pipe system setup for the experimental tests

J. Hydraul. Eng., 2017, 143(10): 04017044

Downloaded from ascelibrary.org by Hong Kong University of Sci and Tech (HKUST) on 08/08/17. Copyright ASCE. For personal use only; all rights reserved.

Downloaded from ascelibrary.org by Hong Kong University of Sci and Tech (HKUST) on 08/08/17. Copyright ASCE. For personal use only; all rights reserved.

Fig. 7. (Color) Part of the experimental pipe system setup (image by Moez Louati)

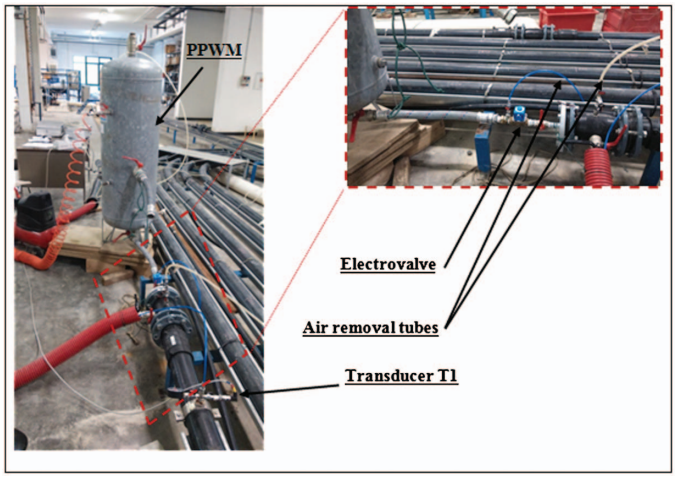

Fig. 8. (Color) Portable pressure wave maker and its connection to the pipe via the electrovalve (images by Moez Louati)

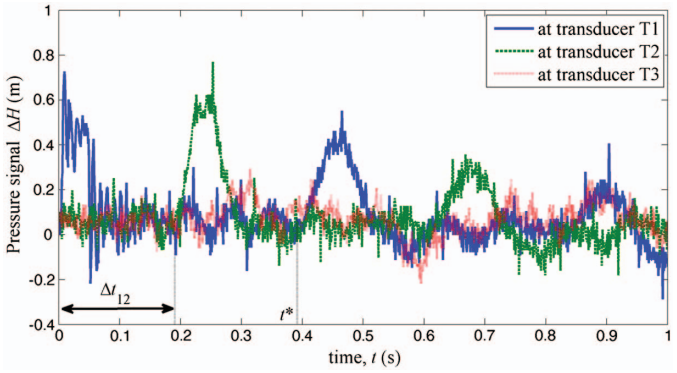

Fig. 9. (Color) Pressure signal ($\Delta H = H_T - H_{T,0}$) acquired at Sections T1, T2, and T3

has been simulated using the method of characteristics (MOC) (Wylie et al. 1993). In the one-dimensional numerical model, neither unsteady friction nor viscoelasticity effects have been considered; furthermore, a constant value of the pressure wave speed has been assumed. To simulate the EV boundary condition in the one-dimensional numerical code, the experimental pressure signal (e.g., the one at T1 reported in Fig. 9) is imposed at the downstream valve location, until the arrival of the first pressure wave reflected

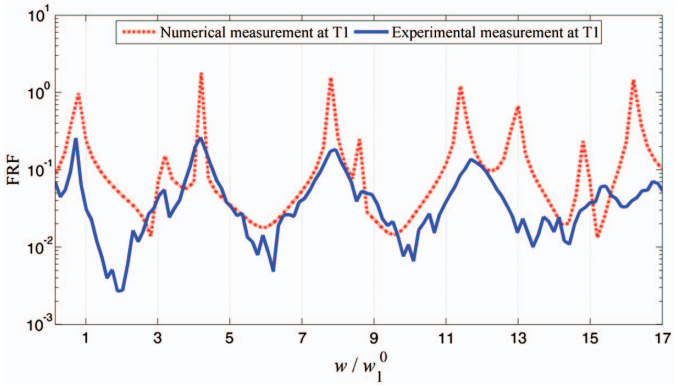

Fig. 10. (Color) Frequency response function of the pressure signal measured at Section T1 for Setup 1 (blockage length $\eta_2 \approx 0.156$): comparison between experimental and numerical results

from the blockage (t^* in Fig. 9). At $t > t^*$, the downstream boundary condition is modeled as a dead end.

Experimental Results and Discussion

Discussion of Experimental Error

In Fig. 10, the FRF of the pressure signal of Setup 1 (Fig. 9) with $\eta_2 \approx 0.156$ measured at Section T1 is compared with the results of the numerical model. On the frequency axis in Fig. 10, the dimensionless frequency w/w_1^0 is shown with $w_1^0 = [\pi a/(2L)]$ being the first eigenfrequency for the intact RPV system. Fig. 10 shows that the first seven experimental eigenfrequencies capture the main features of those given by the numerical result. In fact, the mean error, i.e., the difference between the numerical and experimental dimensionless frequencies, is approximately 5% for the first five modes and approximately 20% for the sixth and seventh modes. This good result is obtained notwithstanding the restrictive assumptions of the numerical model—both unsteady friction and (more important) the viscoelasticity are not taken into account (Meniconi et al. 2012)—and some clearly visible differences between the plotted results for the actual pipe system and the model simulation.

Differences between the experimental and model results arise first because the pipe has been assumed to be straight without accounting for bend effects. The mean distance between two successive bends is approximately $l_{\text{bend}} \approx 10$ m. If wave reflection and transmission between the bends has a Bragg-type resonance effect, then the influence of these bends may be expected to become apparent at frequencies close to $2\pi a/(4 \cdot l_{\text{bend}})]/w_1^0 = [\pi a/(2 \cdot 10)]/w_1^0 \approx 15$ [Eq. (4)]. Hence this may affect the eigenfrequencies at the sixth mode and higher. Second, fluid–structure interactions have been neglected. However, the pipe anchorage effect is likely small because the applied probing transient pressure signal is small [less than 1 m (Fig. 9)], and therefore the resulting pipe displacement is also small. Eigenfrequencies at higher modes (>7) are not as reliable in any case because of the noise and errors and the limited frequency bandwidth (FBW). Moreover, because the full-scale pressure probe is still large compared with the maximum value of the pressure, the accuracy of the acquired pressure signals are not as high as they might be with a transducer set to an even smaller measurement range.

The last, and perhaps most significant source of error concerns the evaluation of the pressure wave speed. Several factors may influence actual wave speed versus the assumed average or constant wave speeds used in the analyses presented in this

paper: (1) pressure wave speed of the blockage section is different from that for the blockage-free pipe because of the different diameter and pipe wall thickness, (2) the assumption of constant pressure wave speed in polymeric pipes may be inaccurate and is the subject of ongoing discussion arising from experimental results (Covas et al. 2005; Mitosek and Chorzelski 2003), and (3) the mean wave speed ($a = 355$ m/s) is based on the average of 16 samples (repeated experiments) with a standard deviation of 15 m/s. To provide a reference point about the significant error contribution from uncertainty in the actual wave speed, it can be stated that an error of 4% in the value of a produces a corresponding error in the eigenfrequency estimates that increases almost linearly from 4% at the first mode to 63% at the seventh mode; whereas an error of 1% in wave speed produces an error in the eigenfrequency that increases almost linearly from 0.9% at the first mode to 14% at the seventh mode.

Setup 1: Extended Blockage

Fig. 11 gives the FRF of the pressure signal for the case of blockage length $\eta_2 \approx 0.156$ (see Setup 1 in Table 1) measured at T1 (downstream boundary). Fig. 11 indicates the location of maximum reflection frequencies (w_n^R) and total transmission frequencies (w_n^T) [Eqs. (4) and (5)]. Fig. 11 shows that the third and fourth resonant frequencies, located respectively at $w/w_{10} \approx 4.2$ and $w/w_{10} \approx 8$, experience relatively large shift with respect to the eigenfrequencies of the intact system (indicated by vertical dashed lines in Fig. 11). This is because these eigenfrequencies are close to the first Bragg resonance frequency of maximum reflection ($w_1^R/w_1^0 \approx 6.4$) (Fig. 11) where the blocked pipe system behaves as if the blockage is located at the boundary with a modified area ratio $\bar{\alpha} = \alpha^2$, and therefore why the shift is quite large (Fig. 4). On the other hand, the seventh eigenfrequency, located at $w/w_1^0 \approx 13.1$, is close to the first Bragg resonance frequency of total transmission ($w_1^T/w_1^0 \approx 12.8$) (Fig. 11), and therefore the seventh eigenfrequency experiences almost zero shift as expected from Fig. 4.

A special feature occurred in Fig. 11. This feature is that the second eigenfrequency, although close enough to the first Bragg resonance frequency of maximum reflection, is not shifted with respect to the second eigenfrequency of the intact pipe case. This is explained by the fact that the blockage is placed at a zero-shift location [Eq. (7)]. In fact, blockage location $\eta_3 + \eta_2/2 = (76.75 + 24/2)/153.61 = 0.5778$ is very close to the second shift location given by Eq. (7) as follows:

$$\eta_3 + \frac{\eta_2}{2} = \{0.1048 \text{ or } 0.5619 \text{ or } 0.7715\} \tag{16}$$

If Eq. (8), which gives the zero-shift locations for shallow blockage case, is used instead of Eq. (7), the possible blockage locations become

$$\eta_3 + \frac{\eta_2}{2} = \{0.1667 \text{ or } 0.5000 \text{ or } 0.8333\} \tag{17}$$

Eq. (17) shows that the second possible blockage location is close to the true blockage location (0.5778) with approximately 7.8% error. The error between the possible blockage locations given by Eqs. (16) and (17) is approximately 6%. This shows that when a zero shift is observed in the FRF, it gives a narrow set of possible blockage locations. Such information has never been exploited before, which actually could improve the efficiency of inverse transient-based blockage-detection methods.

Fig. 11 shows that significant shifts (i.e., $\Delta w_m/w_1^0 \approx 1$) occur at the third and fourth eigenfrequencies, with the third eigenfrequency shift being negative and the fourth eigenfrequency shift being positive. In these cases, assuming that those shifts correspond

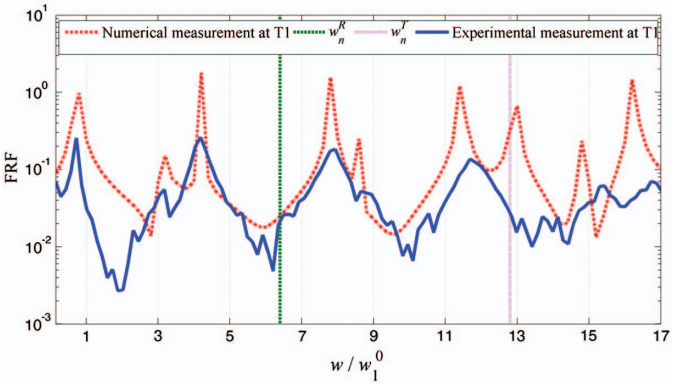

Fig. 11. (Color) Frequency response function of the pressure signal measured at T1 for the test case with blockage length $\eta_2 \approx 0.156$ (Setup 1 in Table 1 with $a = 355$ m/s) indicating the Bragg resonance frequencies

to maximum shifts, Eqs. (11) and (12) for maximum shift locations could be applied, which give

$$\eta_3 + \frac{\eta_2}{2} \in \{0.1414; 0.6195\}; \qquad w_3/w_1^0 = 4.18 \tag{18}$$

and

$$\eta_3 + \frac{\eta_2}{2} \in \{0.31; 0.5633; 0.8165\}; \qquad w_4/w_1^0 = 7.9 \tag{19}$$

Eqs. (18) and (19) show that the blockage location, which is actually at $\eta_3 + \eta_2/2 = 0.5778$, is close to the second negative maximum shift location of the third mode and near the second positive maximum shift location of the fourth mode. This shows that, although a significant shift is used, which is not necessary a maximum shift, Eqs. (11) and (12) could give quite accurate approximation for the blockage location with an error of approximately 1.4–4.2%. Similar to the zero-shift case, this shows that additional information on the blockage location could be obtained from the FRF when a significant shift is observed, which was not exploited before.

A shift is observed at the first eigenfrequency in Fig. 11, where $w_1/w_1^0 = 0.72$. In this case, Eq. (15) for low-frequency approximation, could be used to approximate the first eigenfrequency, which gives

$$\frac{w_1}{w_1^0} \approx \frac{2}{\pi}\sqrt{\frac{\alpha}{\eta_2\eta_3}} = \frac{2}{\pi}\sqrt{\frac{0.168}{0.156 \times 0.5}} = 0.9343 \tag{20}$$

There is a large difference between the experimental and the approximated values (21.4% error). Even based on the numerical results, which give $w_1/w_1^0 = 0.8$, the difference is still large (13% error). Therefore, Eq. (15) does not provide accurate approximation. However, if Eq. (14) is used instead of Eq. (15), the first eigenfrequency is

$$\frac{w_1}{w_1^0} \approx \frac{2}{\pi}\sqrt{\frac{\alpha}{\alpha^2\eta_1\eta_2 + \alpha\eta_1\eta_3 + \eta_2\eta_3}} \approx 0.83 \tag{21}$$

which gives approximately 50% better accuracy (11% error) than Eq. (15). Consequently, Eq. (15) is probably not reliable for real applications, whereas Eq. (14) might give enough accuracy because it produces an error relatively close to the measurement error.

The knowledge of Bragg resonance frequencies informs the blockage characteristics [e.g., blockage length in Eqs. (4) and (5)].

Downloaded from ascelibrary.org by Hong Kong University of Sci and Tech (HKUST) on 08/08/17. Copyright ASCE. For personal use only; all rights reserved.

However, it may not be trivial to identify the Bragg resonance frequencies from the FRF. Nevertheless, Bragg resonance frequency of maximum reflection could be approximated to be the intact pipe system's eigenfrequency at the mode where the first significant positive shift occurs. This is because, as discussed in Louati et al. (2016), positive shift is small at low modes and becomes large only near Bragg resonance frequency of maximum reflection. For example, Fig. 11 shows that the first ($n = 1$) significant positive shift occurs just above the fourth mode of the intact pipe ($w_4/w_1^0 = 7.9$). Therefore, the fourth eigenfrequency of the intact pipe system (w_4^0) could approximated to be the Bragg resonance frequency of maximum reflection. In fact, inserting w_4^0 into Eq. (4) gives

$$\eta_2 = \frac{1}{w_4^0/w_1^0} = \frac{1}{7} = 0.1425 \approx 0.156 \tag{22}$$

which is very close to the true blockage length (Table 1) with approximately $(0.156 - 0.1425) \times 100 = 1.36\%$ error.

Moreover, as mentioned in "Brief Review of Eigenfrequency Shift Mechanism," at modes with eigenfrequency close to the Bragg resonance frequency of maximum reflection, the blocked pipe system becomes equivalent to a junction pipe system (where the blockage is placed at either boundary of the pipe system) with squared blocked area ratio (α^2). Therefore, if a maximum shift at such modes is measured, then Eq. (6) could be used to determine the area ratio (α). For example, using the significant positive shift observed at the fourth mode ($w_4/w_1^0 = 7.9$) (Fig. 11), Eq. (6) gives

$$\alpha = \sqrt{\frac{1 + \sin[7.9\pi/2(1 - 0.1425)]}{1 - \sin[7.9\pi/2(1 - 0.1425)]}} = 0.1792 \approx 0.168 \tag{23}$$

which is very close to the true area ratio with approximately $(0.1792 - 0.168) \times 100 = 1.12\%$ error.

Setup 2: Short Blockage

Fig. 12 gives the FRF of the pressure signal measured at T1 (downstream boundary) for the test case with blockage length $\eta_2 \approx 0.027$ (see Setup 2 in Table 1). Fig. 12 provides a comparison between experimental and numerical results and shows relatively good fitting between them. In this case, the Bragg resonance frequencies are too high ($w_1^R/w_1^0 = 37$) to be observed in the frequency domain due to the limitation of the injected FBW. In fact, Fig. 12 shows that all measured eigenfrequency shifts are either nearly zero or negative shifts. This because positive shifts start to occur only at modes with eigenfrequencies close to the Bragg resonance frequency of maximum reflection ($w_1^R/w_1^0 = 37$) (Louati and Ghidaoui 2016b).

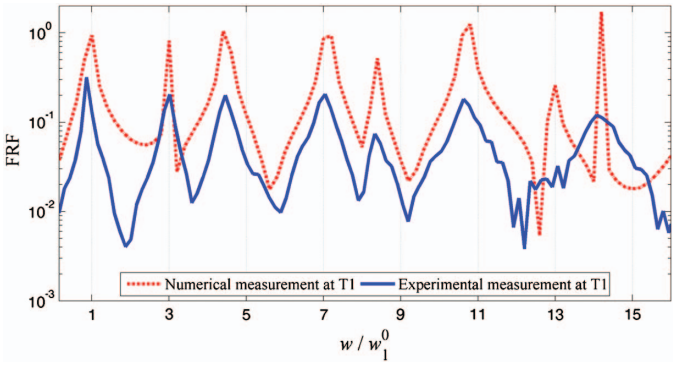

Fig. 12. (Color) Frequency response function of the pressure signal measured at T1 for the test case with blockage length $\eta_2 \approx 0.027$ (Setup 2 in Table 1 with $a = 370$ m/s) indicating the comparison between experimental and numerical results

Zero shift is observed at the second and fourth eigenfrequencies (Fig. 12). Therefore, with known α, Eq. (7) could be applied to obtain sets of possible blockage locations. A quick calculation shows that $\eta_3 + \eta_2/2 = (76.75 + 3.6/2)/133.21 = 0.5897$, whereas the sets of blockage locations at the second and fourth modes from Eq. (7) are

$$\eta_3 + \frac{\eta_2}{2} = \{0.0834; 0.5833; 0.7501\} \tag{24}$$

and

$$\eta_3 + \frac{\eta_2}{2} = \left\{ \begin{matrix} 0.0374; 0.2484; 0.3231; 0.5341; \\ 0.6088; 0.8198; 0.8945 \end{matrix} \right\} \tag{25}$$

respectively.

Eqs. (24) and (25) show that the blockage midlength is located near the second and fourth zero-shift position of the second and fourth modes, respectively. Again, If there is no prior knowledge of the blockage characteristics (i.e., η_2 and α), then Eq. (8), which gives the zero-shift locations for shallow blockage case, is used instead of Eq. (7), introducing an error between 3.5 and 8.5%.

Fig. 12 shows that significant negative shifts occur at the third and fifth eigenfrequencies. Assuming these shifts correspond to maximum shift magnitudes at the given modes, then Eqs. (11) and (12) could be applied and give

$$\eta_3 + \frac{\eta_2}{2} \in \{0.1629; 0.6124\}; w_3/w_1^0 = 4.45 \tag{26}$$

and

$$\eta_3 + \frac{\eta_2}{2} \in \{0.08; 0.32; 0.56; 0.8\}; w_5/w_1^0 = 8.33 \tag{27}$$

Eqs. (26) and (27) show that the blockage location, which is actually at approximately $\eta_3 + \eta_2/2 = 0.59$, is close to the second and third negative maximum shift location of the third and fifth modes with an error of approximately 2.2 and 3%, respectively. Again, this shows that Eqs. (11) and (12) could give quite accurate approximation for the blockage location based on a significant shift magnitude, which may not be necessarily the exact maximum shift magnitude.

The first eigenfrequency shift in Fig. 12 is very small and therefore the low-frequency approximation [Eq. (14) or Eq. (15)] cannot be used for short (discrete) blockage even though the blockage is quite severe.

Unless higher FBW is used to measure eigenfrequency shifts at high modes, the Bragg resonance frequencies could not determined, and by consequence, the blockage characteristics (i.e., η_2 and α) could not be easily obtained as in the extended blockage case (Setup 1) [Eqs. (22) and (23)]. This shows the need of high FBW to obtain better accuracy when detecting multiscale defects in a pipeline using transient methods as mentioned previously in the literature (e.g., Louati and Ghidaoui 2015; Lee et al. 2014).

Conclusions

This paper summarizes the basic theoretical features of the eigenfrequency shift mechanism and validates those features through experimental tests. The key conclusions are as follows:

1. The effect of Bragg resonance on the eigenfrequency shift is observed in the experimental tests. It is shown that, if Bragg resonance frequency of maximum reflection is identified, then

Downloaded from ascelibrary.org by Hong Kong University of Sci and Tech (HKUST) on 08/08/17. Copyright ASCE. For personal use only; all rights reserved.

the blockage length could be approximated accurately with approximately 1% error. If, in addition, a significant shift is measured at the Bragg resonance frequency of maximum reflection, the blockage area could be determined by approximating the blocked system by a junction system.

2. The relation between zero-shift and blockage location [Eq. (7)] is validated experimentally. The results show that the occurrence of zero shift in the FRF yields a discrete set of possible blockage locations. Identification of this set of feasible blockage locations enormously reduces the search domain space for inverse optimization techniques used for transient-based blockage detection. Shallow blockage approximation [Eq. (8)] could be used for the zero-shift location with an error of approximately 6% at low modes (e.g., $m = 2$). This error is lower for zero-shift locations at high modes.
3. The experimental results show that even for shifts that may not necessarily be the maximum shift magnitude, the relation between maximum shift magnitude and blockage location [Eq. (11)] still gives accurate results with an error of approximately 1–4%.
4. Low-frequency approximation is tested experimentally. The results show that the Helmholtz resonance frequency [Eq. (15)] is probably not reliable for real applications (>20% error), whereas Eq. (14) might provide better accuracy because it produces an error relatively close to the measurement errors (approximately 10% error).
5. Conclusions 1–4 show how an improved understanding of the eigenfrequency shift mechanism provides a direct means for extracting additional information from the FRF. This additional information can significantly improve the efficiency of the existing transient-based techniques for blockage detection in pipe systems.
6. Probably the most important error affecting the experimental results is the measurement error of wave speed. It is found that an error of 4% in wave speed produces an error in the eigenfrequency estimates that increases almost linearly from 4% at the first mode to 63% at the seventh mode.

Acknowledgments

This study is supported by the Hong Kong Research Grant Council (Projects 612712, 612713, and T21-602/15R), by the Postgraduate Studentship, the University of Perugia, the Italian Ministry of Education, University and Research (MIUR)—under the Projects of Relevant National Interest "Advanced analysis tools for the management of water losses in urban aqueducts" and "Tools and procedures for an advanced and sustainable management of water distribution systems"—and Fondazione Cassa Risparmio Perugia, under the project "Hydraulic and microbiological combined approach toward water quality control (No. 2015.0383.021)." The authors thank Dr. D.A. McInnis for the technical and editorial suggestions.

Notation

The following symbols are used in this paper:

A_0 = area of intact pipe (m^2);
A_2 = area of Pipe 2 (the blocked region in the pipe) (m^2);
a = acoustic wave speed in water ($m\,s^{-1}$);
$H_{P,0}$ = initial pressure head in the PPWM (m);
H_{ST} = supply pressure head (m);
$H_{T1,0} = H_{T2,0} = H_{T3,0}$ = initial pressure head at Transducers T1, T2, T3, respectively (m);
k = wave number (m^{-1});
L = whole pipe length (m);
l_1 = length of Pipe 1 (m);
l_2 = length of Pipe 2 (m);
l_3 = length of Pipe 3 (m);
m = resonant mode number for pipe system of length L;
t = time (s);
t^* = arrival time of the first pressure wave reflected by the blockage;
w = angular frequency ($rad\,s^{-1}$);
w_m = mth resonant frequencies in the blocked pipe case ($rad\,s^{-1}$);
$w_m^{\max}$ = maximum eigenfrequency measures at the mth mode ($rad\,s^{-1}$);
w_n^R = Bragg resonance frequency of maximum reflection ($rad\,s^{-1}$);
w_m^T = Bragg resonance frequency of maximum reflection ($rad\,s^{-1}$);
w_m^0 = mth resonant frequencies in the intact pipe case ($rad\,s^{-1}$);
x = axial coordinate (m);
α = area ratio between A_2 and A_0;
Δw_m = mth eigenfrequency shift; and
$\eta_j = l_j/L$ dimensionless length.

References

ASCE. (2013). *Report card on infrastructure*, Reston, VA.
Brunone, B., Ferrante, M., and Meniconi, S. (2008a). "Discussion of detection of partial blockage in single pipelines." *J. Hydraul. Eng.*, 10.1061/(ASCE)0733-9429(2008)134:6(872), 872–874.
Brunone, B., Ferrante, M., and Meniconi, S. (2008b). "Portable pressure wave-maker for leak detection and pipe system characterization." *J. Am. Water Works Assn.*, 100(4), 108–116.
Chaudhry, M. H. (2014). *Applied hydraulic transients*, 3rd Ed., Springer, New York.
Coelho, B., and Andrade-Campos, A. (2014). "Efficiency achievement in water supply systems—A review." *Renewable Sustainable Energy Rev.*, 30, 59–84.
Colombo, A. F., and Karney, B. W. (2002). "Energy and costs of leaky pipes: Toward comprehensive picture." *J. Water Resour. Plann. Manage.*, 10.1061/(ASCE)0733-9496(2002)128:6(441), 441–450.
Covas, D., Stoianov, I., Mano, J. F., Ramos, H., Graham, N., and Maksimovic, C. (2005). "The dynamic effect of pipe-wall viscoelasticity in hydraulic transients. II: Model development, calibration and verification." *J. Hydraul. Res.*, 43(1), 56–70.
De Salis, M. H. F., and Oldham, D. J. (1999). "Determination of the blockage area function of a finite duct from a single pressure response measurement." *J. Sound Vib.*, 221(1), 180–186.
Domis, M. A. (1979). "Acoustic resonances as a means of blockage detection in sodium cooled fast reactors." *Nucl. Eng. Des.*, 54(1), 125–147.
Domis, M. A. (1980). "Frequency dependence of acoustic resonances on blockage position in a fast reactor subassembly wrapper." *J. Sound Vib.*, 72(4), 443–450.
Duan, H., Lee, P. J., Ghidaoui, M. S., and Tung, Y. (2011). "Extended blockage detection in pipelines by using the system frequency response analysis." *J. Water Resour. Plann. Manage.*, 10.1061/(ASCE)WR.1943-5452.0000145, 55–62.
Duan, H., Lee, P. J., Kashima, A., Lu, J., Ghidaoui, M., and Tung, Y. (2013). "Extended blockage detection in pipes using the system frequency response: Analytical analysis and experimental verification." *J. Hydraul. Eng.*, 10.1061/(ASCE)HY.1943-7900.0000736, 763–771.
El-Rahed, M., and Wagner, P. (1982). "Acoustic propagation in rigid ducts with blockage." *J. Acoust. Soc. Am.*, 72(3), 1046–1055.

Downloaded from ascelibrary.org by Hong Kong University of Sci and Tech (HKUST) on 08/08/17. Copyright ASCE. For personal use only; all rights reserved.

EURAMET (European Association of National Metrology Institutes). (2011). "Guidelines on the calibration of electromechanical manometers." ⟨http://dastmardi.ir/Guides/EURAMET_cg-17__v_2.0_Electromechanical_Manometers.pdf⟩.

Fant, G. (1975). "Vocal-tract area and length perturbations." *STL-QPSR, 4/1975*, Speech Transmission Laboratory, Dept. of Speech Communication, Royal Institute of Technology, Stockholm, Sweden, 1–14.

Heinz, J. (1967). "Perturbation functions for the determination of vocal-tract area functions from vocal-tract eigenvalues." *STL-QPSR, 1/1967*, Speech Transmission Laboratory, Dept. of Speech Communication, Royal Institute of Technology, Stockholm, Sweden, 1–14.

Lee, P. J., Duan, H., Tuck, J., and Ghidaoui, M. (2014). "Numerical and experimental study on the effect of signal bandwidth on pipe assessment using fluid transients." *J. Hydraul. Eng.*, 10.1061/(ASCE)HY.1943-7900.0000961, 04014074.

Louati, M. (2016). "In-depth study of plane wave-blockage interaction and analysis of high frequency waves behaviour in water-filled pipe systems." Ph.D. dissertation, Hong Kong Univ. of Science and Technology, Hong Kong, ⟨http://lbezone.ust.hk/bib/b1618552⟩.

Louati, M., and Ghidaoui, M. S. (2015). "Role of length of probing waves for multi-scale defects detection in pipes." *Proc., 36th IAHR Congress*, The Hague, Netherlands.

Louati, M., and Ghidaoui, M. S. (2016a). "Eigenfrequency shift mechanism due to an interior blockage in a pipe." *J. Hydraul. Eng.*, in press.

Louati, M., and Ghidaoui, M. S. (2016b). "In-depth study of the eigenfrequency shift mechanism due to variation in the cross sectional area of a conduit." *J. Hydraul. Res.*, in press.

Louati, M., Ghidaoui, M. S., Meniconi, S., and Brunone, B. (2016). "Bragg-type resonance in blocked pipe system and its effect on the eigenfrequency shift." *J. Hydraul. Eng.*, in press.

MATLAB [Computer software]. MathWorks, Natick, MA.

Meniconi, S., Brunone, B., and Ferrante, M. (2011a). "In-line pipe device checking by short period analysis of transient tests." *J. Hydraul. Eng.*, 10.1061/(ASCE)HY.1943-7900.0000309, 713–722.

Meniconi, S., Brunone, B., and Ferrante, M. (2012). "Water-hammer pressure waves interaction at cross-section changes in series in visco-elastic pipes." *J. Fluids Struct.*, 33, 44–58.

Meniconi, S., Brunone, B., Ferrante, M., and Capponi, C. (2016). "Mechanism of interaction of pressure waves at a discrete partial blockage." *J. Fluids Struct.*, 62, 33–45.

Meniconi, S., Brunone, B., Ferrante, M., and Massari, C. (2011c). "Small amplitude sharp pressure waves to diagnose pipe systems." *Water Resour. Manage.*, 25(1), 79–96.

Meniconi, S., Duan, H., Lee, P., Brunone, B., Ghidaoui, M., and Ferrante, M. (2013). "Experimental investigation of coupled frequency and time-domain transient test–based techniques for partial blockage detection in pipelines." *J. Hydraul. Eng.*, 10.1061/(ASCE)HY.1943-7900.0000768, 1033–1040.

Mermelstein, P. (1967). "Determination of the vocal-tract shape from measured formant frequencies." *J. Acoust. Soc. Am.*, 41(5), 1283–1294.

Milenkovic, P. (1984). "Vocal tract area functions from two point acoustic measurements with formant frequency constraints." *IEEE Trans. Acoust. Speech Signal Process.*, 32(6), 1122–1135.

Milenkovic, P. (1987). "Acoustic tube reconstruction from noncausal excitation." *IEEE Trans. Acoust. Speech Signal Process.*, 35(8), 1089–1100.

Mitosek, M., and Chorzelski, M. (2003). "Influence of visco-elasticity on pressure wave velocity in polyethylene MDPE pipe." *Archit. Hydro. Eng. Environ. Mech.*, 50(2), 127–140.

Qunli, W., and Fricke, F. (1989). "Estimation of blockage dimensions in a duct using measured eigenfrequency shifts." *J. Sound Vib.*, 133(2), 289–301.

Qunli, W., and Fricke, F. (1990). "Determination of blocking locations and cross-sectional area in a duct by eigenfrequency shifts." *J. Acoust. Soc. Am.*, 87(1), 67–75.

Schroeder, M. R. (1967). "Determination of the geometry of the human vocal tract by acoustic measurements." *J. Acoust. Soc. Am.*, 41(4B), 1002–1010.

Schroeter, J., and Sondhi, M. M. (1994). "Techniques for estimating vocal-tract shapes from the speech signal." *IEEE Trans. Speech Audio Process.*, 2(1), 133–150.

Sondhi, M. M., and Gopinath, B. (1971). "Determination of vocal-tract shape from impulse response at the lips." *J. Acoust. Soc. Am.*, 49(6B), 1867–1873.

Sondhi, M. M., and Resnick, J. (1983). "The inverse problem for the vocal tract: Numerical methods, acoustical experiments, and speech synthesis." *J. Acoust. Soc. Am.*, 73(3), 985–1002.

Stephens, M. (2008). "Transient response analysis for fault detection and pipeline wall condition assessment in field water transmission and distribution pipelines and networks." Ph.D. thesis, Univ. of Adelaide, Adelaide, Australia.

Stevens, K. N. (1998). *Acoustic phonetics*, MIT Press, London.

Wylie, E. B., Streeter, V. L., and Suo, L. (1993). *Fluid transients in systems*, Prentice Hall, Englewood Cliffs, NJ.

Downloaded from ascelibrary.org by Hong Kong University of Sci and Tech (HKUST) on 08/08/17. Copyright ASCE. For personal use only; all rights reserved.